ENERGY TRANSFER WITHIN A PERTURBED PLANE WALL JET

Ebenezer P. Gnanamanickam
Department of Aerospace Engineering
Embry-Riddle Aeronautical University
Daytona Beach, FL, USA
gnanamae@erau.edu

Shibani Bhatt
Department of Aerospace Engineering
Embry-Riddle Aeronautical University
Daytona Beach, FL, USA

Sravan Artham
Department of Aerospace Engineering
Embry-Riddle Aeronautical University
Daytona Beach, FL, USA

ABSTRACT

The energy transfer within a perturbed plane wall jet developing in still air is studied using complementary hot-wire anemometry and time resolved, particle image velocimetry measurements. The perturbation was observed to reduce the outer velocity scale while increasing the outer length scale. The friction velocity was reduced due to the perturbation at all streamwise locations considered. The energy spectra of the perturbed and unperturbed flow revealed that the perturbation increased the energy of the large-scales in the wall region of the plane wall jet. However, the size of these recipient large-scales corresponded to that of the large-scales in the outer free-shear region. This energy transfer occurred consistently irrespective of the direction of the transfer. The linear response of the flow due to the perturbation along with changes to the turbulence intensities, production and dissipation rates are also presented and discussed.

INTRODUCTION

A plane wall jet (PWJ) is formed when fluid exits a high aspect ratio rectangular nozzle along a flat plate. The resulting flow field has a free-shear like flow in its outer extremities with a boundary layer in the inner region (Launder & Rodi, 1981, 1983; Wygnanski *et al.*, 1992; Schneider & Goldstein, 1994; Abrahamsson *et al.*, 1994; Rostamy *et al.*, 2011). This unique configuration of the PWJ leads to the formation of energetic large-scale structures in the outer free-shear region (Katz *et al.*, 1992). Hence, the inner boundary layer is growing in the presence of the outer free-shear layer structure. The structures in the inner wall region and the outer free-shear region are also interacting with each other (Dejoan & Leschziner, 2005; Banyassady & Piomelli, 2015). This interaction occurs over an interaction zone or region. In this region the turbulent production is low and the kinetic energy balance shows that turbulent transport and convection primarily balance dissipation (Dejoan & Leschziner, 2005). Thus the PWJ is a non-canonical wall-bounded flow where a natural and complex interaction exists between the outer free-shear layer and the inner boundary layer.

Large-scale perturbations of canonical boundary layers (the zero-pressure gradient boundary layer) have recently been carried out to understand the embedded, non-linear mechanisms within wall layers (Jacobi & McKeon, 2011*a*,*b*; Duvvuri & McKeon, 2016, 2015). In this context, controlled perturbations can be introduced into the PWJ via acoustic perturbation in the settling chamber. The unique configuration of the PWJ is exploited in the present study to study the energy transfer mechanisms within complex wall-bounded flows, where a natural interaction exists between the inner boundary layer and energetic outer layer structures. Such an approach has been previously followed by Wygnanski and colleagues (Katz *et al.*, 1992; Zhou *et al.*, 1993, 1996) and Schober & Fernholz (2000). Katz *et al.* (1992) carried out a parametric study on a perturbed PWJ over a range of Reynolds numbers ($Re_j = bV_j/\nu = 3000$ to 30000) and Strouhal numbers ($St = f_f b/V_j = 3.4\times10^{-3}$ to 18.3×10^{-3}). Here, V_j is the PWJ exit centerline velocity, f_f the forcing frequency and ν the kinematic viscosity. They determined that the production in the near-wall region was reduced by the forcing with a concomitant reduction in wall shear stress exceeding 30%.

In an associated study Zhou *et al.* (1996) acoustically perturbed a PWJ in the presence of an external stream. The PWJ Reynolds number $Re_j = 6900$ and the forcing was at a single Strouhal number of $St = 9.5\times10^{-3}$. The forcing frequency f_f was chosen to be the predominant frequency in the wall region of the unperturbed PWJ at a downstream location of approximately $x/b = 100$. They determined that the wall shear stress was reduced by about 7% between streamwise distances $x/b = 100$ and 200. There was also a significant increase in the near-wall streamwise turbulence intensity when $x/b < 100$ which reduced at further downstream distances along with an increase in streamwise turbulence intensity away from the wall. They interpreted these two observations as a transfer of energy from the wall outwards.

Schober & Fernholz (2000) also studied a forced PWJ at a Reynolds number $Re_j = 10000$. They used a still wire at the PWJ exit to break up the outer large-scales and reduced the wall shear stress while an oscillating wire (estimated Strouhal number $St = 74.6 \times 10^{-3}$) enhanced the outer layer structures with an associated reduction in wall shear-stress.

In the present study we consider a perturbed PWJ developing in still air. In contrast to the work of Zhou *et al.* (1996) the forcing wavelength chosen here is larger than the most energetic large-scales in the flow at the most upstream locations. Hence, as the PWJ develops downstream the energetic large-scales in the flow that are initially smaller than the perturbation wavelength, become equal to and eventually larger than the perturbation wavelengths. This leads to an interesting energy transfer mechanism which is presented here.

EXPERIMENTAL APPROACH

Measurements were carried out in a PWJ facility (see figure 1) where air from a centrifugal fan passes through a series of screens before entering a plenum settling chamber. Following the plenum, air passes through a honeycomb layer, into a two-dimensional contraction of ratio 16:1. The flow then exits through a rectangular nozzle of width $b = 5$ mm at an aspect ratio of 128. Downstream of the PWJ exit, a 12.7 cm long strip of sand paper is installed across the facility floor which trips the boundary layer. The trip was used to minimize the influence of the perturbation on the inner boundary layer transition. All measurements were carried out at a nominal jet Reynolds number $Re_j = bV_j/\nu \approx 5960$. Perturbations were produced by a speaker in the plenum chamber. Results are presented here when the perturbation was at a nominal Strouhal number $St = f_f b/V_j \approx 2 \times 10^{-3}$. In terms of the outer scales the perturbation wavelength $\lambda_{xf} \approx 6.6\delta$ (based on the outer scales at the downstream location $x/b = 137$). The outer velocity scale of the PWJ is the maximum mean velocity U_m while the outer length scale δ is the wall-normal location in the outer jet portion of the PWJ where the velocity is half the maximum mean velocity. The perturbation increased the turbulence intensity at the PWJ exit centerline from $< 1\%$ to 5.5%. Hence, the perturbation is considered large-amplitude perturbation.

Hot-wire anemometry (HWA) based measurements were carried out at several streamwise locations ranging from $x/b = 1$ to $x/b = 162$. Boundary-layer type hot-wire sensors with diameter d =2.5 µm and a nominal aspect ratio $l/d = 200$ were used. To fully resolve the energy of the largest scales in the flow the sampling period was ensured to be $T > 15000\ \delta/U_m$ (Hutchins *et al.*, 2009). Complementary time-resolved particle image velocimetry measurements (PIV) were also carried out centered at a nominal downstream location $x/b = 137$. A single wall-normal slice of temporally resolved measurements were carried out, akin to an array of synchronous hot-wire measurements. It is noted that the wall-normal mean velocity $\overline{w}$ in a PWJ is nonzero hence HWA based measurements measure an effective velocity (U) while the PIV based measurements measures both components of the velocity in the wall-normal-spanwise plane (u and w). Here the wall-normal ordinate is z and the streamwise ordinate is x. The PIV based measurements were mosaiced from two cameras at different magnifications. The nominal final interrogation window size for the bottom camera (focused on the inner boundary layer) was $\Delta z^+ \times \Delta x^+ \approx 4 \times 4$ while that of the top camera was $\Delta z^+ \times \Delta x^+ \approx 6 \times 6$. Here, the superscript $^+$ indicates normalization with respect to viscous or inner units. The friction velocity U_τ was measured using careful near-wall velocity measurements (hot-wire based) and subsequently fitting with a direct numerical simulation based velocity profile. The superscript 0 is used to identify unperturbed quantities. The wall-normal location of the maximum mean velocity $U(z_m) = U_m$ is used to broadly separate the flow into an inner, wall region ($z < z_m$) and an outer, free-shear region ($z > z_m$) for the purpose of the following discussion.

RESULTS

The downstream development of the PWJ with and without perturbation is shown in figure 2. Shown is the mean effective streamwise velocity as measured by HWA and the corresponding turbulence intensity profiles. In the case of perturbed and unperturbed flow the maximum mean velocity U_m (outer velocity scale) is seen to decrease with downstream distance. However, this decrease is more rapid in the case of the perturbed flow. There is also a corresponding increase in the outer length scale δ with increasing downstream distance. This increase is more rapid in the case of the perturbed flow, indicative of enhanced spreading of the PWJ due to perturbation. Together, the increase in δ and the decrease in U_m results in lower momentum closer to the wall. This causes a decrease in friction velocity U_τ at all streamwise locations considered. This decrease increased from about 3.0% at $x/b = 75$ to 7.3% at $x/b = 162$.

There are two peaks in the streamwise turbulence intensity in the case of the PWJ. There is an inner peak which occurs around $z^+ \approx 15$ similar to that seen in canonical boundary layers (for example the zero pressure gradient boundary layer). However, there also exists a peak in the streamwise turbulence intensity in the outer free-shear layer. As the PWJ develops downstream both these peaks reduce in magnitude for both the perturbed and the unperturbed flow. However, at a given streamwise location the effect of perturbation is to increase the overall turbulence intensity. This increase is substantial in the case of the inner peak with a smaller increase in the outer peak.

The turbulence intensity as measured using HWA reflects an effective quantity. The individual Reynolds stresses of the perturbed and unperturbed flow as measured using PIV are shown in figure 3. The increase in inner-normalized turbulence intensity of the streamwise velocity $\sqrt{\overline{u'^2}}$ upon perturbation is seen. This increase occurs primarily in the inner wall layer with a smaller increase in the outer layer. In the inner wall layer, there is no change in the inner-normalized turbulence intensity of the wall-normal velocity $\sqrt{\overline{w'^2}}$ when perturbed. However, in the outer layer the wall-normal turbulence intensity increases due to the imposed perturbation. In the case of the inner-normalized Reynold shear stress $\overline{u'w'}$ there is also no change in the wall region with an increase in the outer free-shear region. This suggests that the changes due to the perturbation are inactive, in that they increase the streamwise turbulence intensity without changes to the wall layer Reynolds shear stress.

The linear response of the PWJ due to the applied perturbation $U_f(\theta_f, z)$, as a function of downstream distance, is shown in figure 4. These are based on phase-locked HWA measurements. At all streamwise locations the wall layer response is a forward leaning flow structure which are similar to the naturally occurring forward leaning structures observed in canonical boundary layers (Tutkun *et al.*, 2009). Such forward leaning structures have also been observed to occur naturally in the wall region of the PWJ (Banyassady & Piomelli, 2014). In the outer free-shear region a struc-

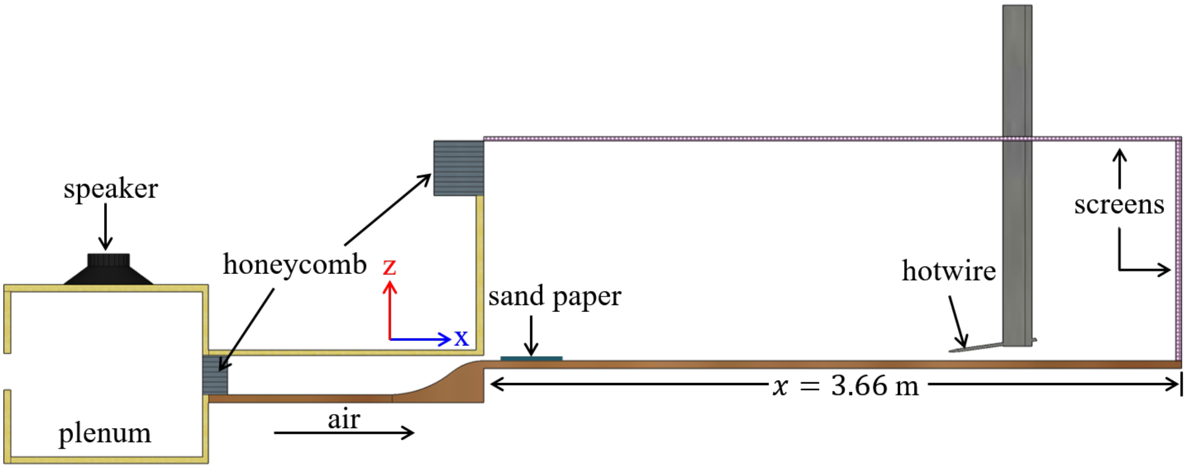

Figure 1. Schematic of the experimental set up.

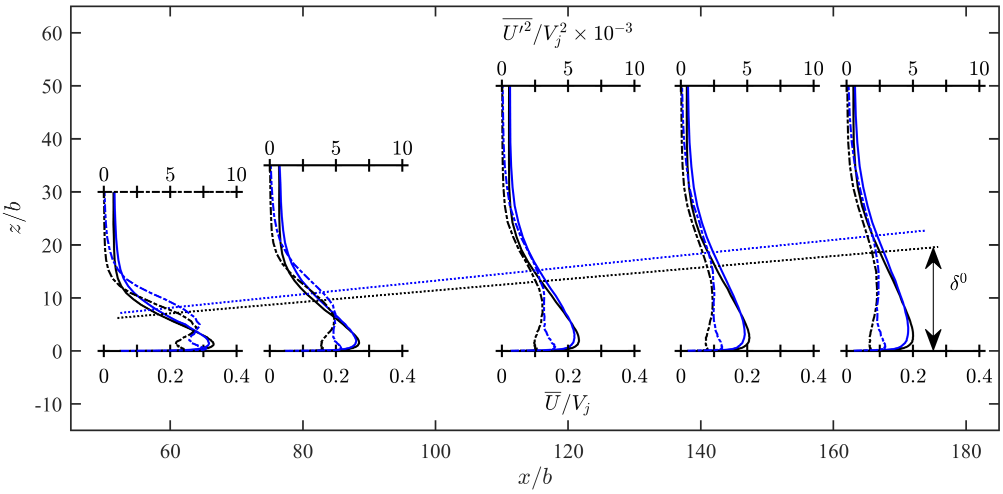

Figure 2. The solid lines show the mean effective streamwise velocity profile ($\overline{U}$) as measured by HWA as the flow develops downstream of the PWJ exit. The dot-dashed line shows the corresponding evolution of the effective streamwise turbulence intensity ($\overline{U'^2}$) profile. The black lines are those corresponding to the unperturbed PWJ while the blue ones are those corresponding to the perturbed PWJ. Both sets of profiles are normalized by the PWJ jet exit velocity V_j. These measurements were carried out using HWA and hence reflect an effective velocity. The development of the outer length scale δ is also shown indicating the spreading rate of the PWJ.

ture that appears to be backward leaning is observed. Backward leaning flow structures in the outer region of the PWJ have also been naturally observed (Banyassady & Piomelli, 2014). At the most downstream locations $x/b > 110$ the linear response appears to show a third structure in the upper extremities of the flow. The linear response structures observed in the perturbed flow at various wall-normal location show a relative phase shift as a function of streamwise distance, indicating that these structures are convecting with different convection velocities.

The changes to the turbulence intensity presents the overall integrated changes due to the perturbation. The spectral changes to the flow as a function of downstream distance is shown in figure 5. The colours are the contours of the pre-multiplied, one-dimensional, streamwise energy spectra $f\phi_{uu}$. The energy spectra is presented as a function of a wavelength $V_j f/b$ and wall-normal distance z, where f are the Fourier frequencies. The unperturbed spectra shows extremely energetic large-scale motions across the entire flow. Here, large-scale motions are broadly defined as flow structures with streamwise wavelength $\lambda_x > 2\delta$, where a frequency is converted to a wavelength using the outer velocity scale. The large-scale energy is concentrated at two different wall-normal locations, one in the wall region and the other in the outer free-shear region. The naturally occurring large-scales in the wall region are referred to as λ_{xw}^n while those in the outer free-shear region are λ_{xj}^n. The perturbation wavelength is referred to as λ_{xf} and is highlighted in figure 5. It is noted that λ_{xj} and λ_{xw}^n are not distinct wavelengths but represent a range of scales and $\lambda_{xj}^n > \lambda_{xw}^n$ (see figure 5).

As the unperturbed PWJ develops downstream the energetic scales of the flow become larger with increasing downstream location i.e., λ_{xw}^n and λ_{xj}^n increase with x/b. However, the perturbation wavelength λ_{xf} is fixed and hence at the most upstream locations ($x/b \leq 110$) $\lambda_{xf} > \lambda_{xj}^n > \lambda_{xw}^n$. Around $x/b \approx 110 - 137$, λ_{xf} approximately equals the peak in λ_{xj}^n and at further downstream location

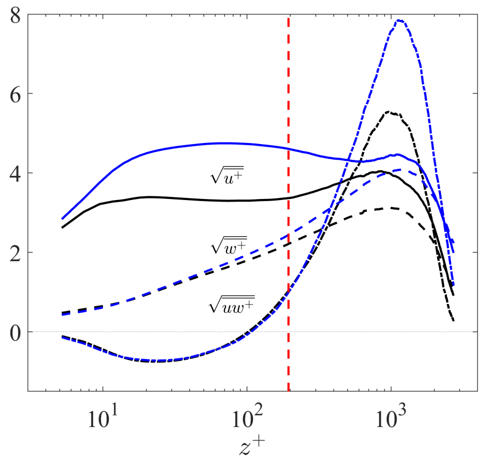

Figure 3. Compares the Reynolds stresses of the perturbed and unperturbed flow. The black lines are those corresponding to the unperturbed flow while the blue ones are those corresponding to the perturbed flow. The line styles are as follows, $\sqrt{\overline{u'^{+2}}}$ (–), $\sqrt{\overline{w'^{+2}}}$ (- - -) and $\overline{u'w'^+}$ (-·-·). The vertical line (- - -) shows the wall-normal location z_m of the maximum velocity U_m corresponding to the unperturbed flow.

λ_{xf} is less than both λ_{xj}^n and λ_{xw}^n. Considering the perturbed spectra it is seen that the excess energy is always transfered to the inner wall region which contains the scalesλ_{xw}^n. However, the recipient wavelengths of the excess perturbation energy $\lambda_{xr} \approx \lambda_{xj}^n$. In other words, the perturbation energy is transferred to a fixed set of scales $\lambda_{xr} \approx \lambda_{xj}^n$ at a fixed wall-normal location, the wall region. This is highlighted in figure 6 where the line plots of $f\phi_{uu}$ of the perturbed flow at two wall-normal locations ($z^+ \approx 15$ and 60) are compared with that of the unperturbed flow at $z \approx 0.6\delta$. Here, the changes due to perturbation in the wall layer is compared with naturally occurring scales in the outer free-shear region. It is observed that the increase in energy occurs in the inner wall region but the recipient scales have a peak that is identical to the outer scales of the unperturbed flow. Hence, at the upstream locations when $\lambda_{xr} < \lambda_{xf}$ the direction of energy transfer is in the manner of a forward cascade while at the downstream locations when $\lambda_{xr} > \lambda_{xf}$ the energy transfer is in the manner of an inverse cascade.

These observations point to interesting mechanisms in the kinetic energy balance. In this context the production P and dissipation rates ε of the perturbed and unperturbed flow are estimated from PIV measurements and presented in figure 7 and 8 respectively. The production was estimated using $P \approx \overline{-uw}\partial\overline{u}/\partial z$ while the dissipation rate was estimated using $\varepsilon \approx 15\nu\overline{(\partial u/\partial x)^2}$. In the case of the unperturbed flow there exists an inner production peak in the wall region much like in canonical boundary layers (see inset of figure 7). However, there is a substantially larger production peak in the outer free-shear region. The effect of perturbation is to decrease slightly the production peak in the wall region with a larger increase in the outer production peak. The dissipation rate shows decreased dissipation in the wall region with an increase in the dissipation rate in the outer free-shear region upon perturbation. Together, these observations suggest a transfer of momentum away from the wall due to the perturbation.

CONCLUSIONS

A PWJ developing in still air was perturbed and the underlying energy transfer mechanism was studied. The perturbation wavelength was chosen to be larger than the energetic large-scale structures naturally occurring in the PWJ. It was observed that the perturbation increased the spreading rate of the PWJ with a decrease in the friction velocity. In the wall region, the perturbation increased the streamwise turbulence intensity with no changes in the wall-normal turbulence intensity or the Reynolds shear stress. The linear response of the PWJ to the perturbation resulted in flow structures similar to naturally occurring flow structures in the wall and free-shear region of the PWJ. The energy spectra revealed that the perturbation energy was transferred to large-scale structures in the wall-region of the PWJ. However, the recipient wavelengths were scales of the size of the outer free-shear layer structures. Thus the energy transfer direction was in the manner of a forward cascade when the perturbation wavelength was larger than the naturally occurring large-scales. This occurred at the most upstream locations. At further downstream locations when the naturally occurring large-scales of the PWJ was larger than the perturbation wavelength the transfer mechanism was in the manner of an inverse cascade. The production in the wall region decreased due to perturbation while increasing in the outer free-shear layer. The dissipation rate also decreased in the wall region while increasing in the outer free-shear layer.

The authors would like to gratefully acknowledge the U.S. Air Force Office of Scientific Research for support of this work through grant FA9550-16-1-0194 managed by Dr. Gregg Abate.

REFERENCES

Abrahamsson, H., Johansson, B & Löfdahl, L. 1994 A turbulent plane two-dimensional wall-jet in a quiescent surrounding. *Eur. J. Mech., B/Fluids* **13**, 533–556.

Banyassady, R. & Piomelli, U. 2014 Turbulent plane wall jets over smooth and rough surfaces. *J. Turb.* **15** (3), 186–207.

Banyassady, R. & Piomelli, U. 2015 Interaction of inner and outer layers in plane and radial wall jets. *J. Turb.* **16** (5), 460–483.

Dejoan, A. & Leschziner, M. A. 2005 Large eddy simulation of a plane turbulent wall jet. *Phys. Fluids* **17** (2), 025102.

Duvvuri, S. & McKeon, B. J. 2015 Triadic scale interactions in a turbulent boundary layer. *J. Fluid Mech.* **767**.

Duvvuri, S. & McKeon, B. J. 2016 Nonlinear interactions isolated through scale synthesis in experimental wall turbulence. *Phys. Rev. Fluids* **1**, 032401.

Hutchins, N., Nickels, T. B., Marušić, I. & Chong, M. S. 2009 Hot-wire spatial resolution issues in wall-bounded turbulence. *J. Fluid Mech.* **635**, 103–136.

Jacobi, I. & McKeon, B. J. 2011*a* Dynamic roughness perturbation of a turbulent boundary layer. *J. Fluid Mech.* **688**, 258.

Jacobi, I. & McKeon, B. J. 2011*b* New perspectives on the impulsive roughness-perturbation of a turbulent boundary layer. *J. Fluid Mech.* **677**, 179–203.

Katz, Y., Horev, E. & Wygnanski, I. 1992 The forced turbulent wall jet. *J. Fluid Mech.* **242**, 577–609.

Launder, B. E. & Rodi, W. 1981 The turbulent wall jet. *Prog. Aerosp. Sci.* **19**, 81–128.

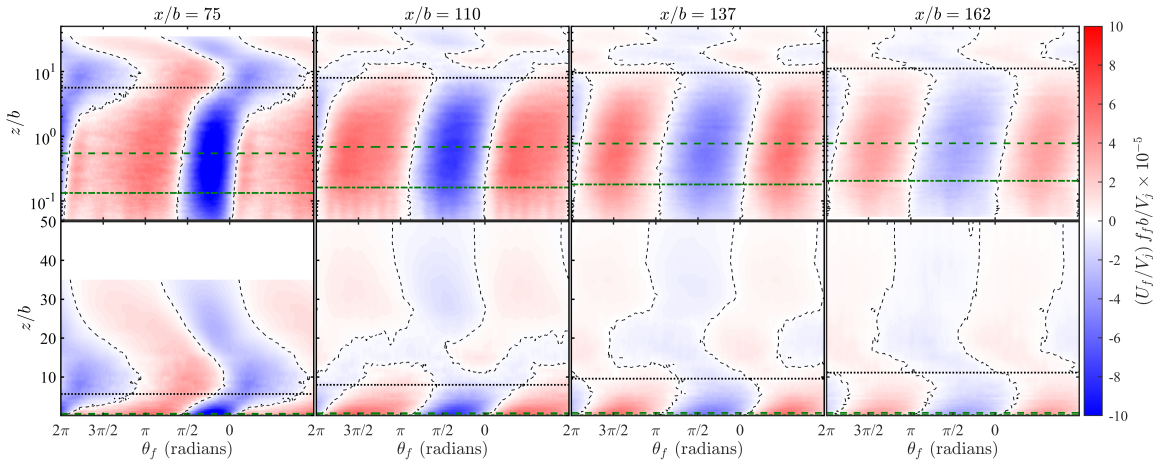

Figure 4. Linear response of the PWJ $U_f(\theta_f, z)$ in logarithmic coordinates (top) and linear coordinates (bottom) is shown. The color represents the magnitude of U_f as indicated by the color bar on the right. The red regions indicate positive fluctuation whereas the blue regions indicate negative fluctuations. The line (- - -) shows $U_f = 0$. The horizontal lines represent the following nominal wall-normal locations, $z^+ \approx 15$ (-·-·), $z^+ \approx 60$ (- - -) and $z \approx 0.6\delta^0$ (- - -) respectively.

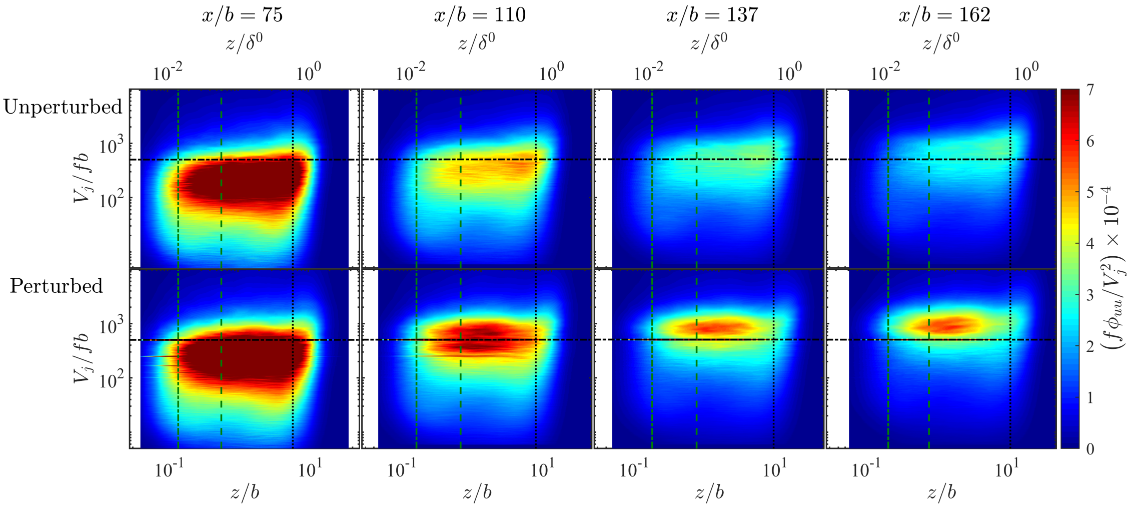

Figure 5. Comparison of the contour maps of the streamwise pre-multiplied energy spectra $f\phi_{uu}/V_j^2$ for the unperturbed (top) and perturbed (bottom) flow. The vertical lines show the wall-normal locations $z^+ \approx 15$ (-·-·), $z^+ \approx 60$ (- - -) and $z \approx 0.6\delta^0$ (······) respectively. The horizontal line (-·-·) is the perturbation wavelength λ_{xf}.

Launder, B. E. & Rodi, W. 1983 The turbulent wall jet measurements and modeling. *Annu. Rev. Fluid Mech.* **15** (1), 429–459.

Rostamy, N., Bergstrom, D. J., Sumner, D. & Bugg, J. D. 2011 The effect of surface roughness on the turbulence structure of a plane wall jet. *Phys. Fluids* **23** (8).

Schneider, M. E. & Goldstein, R. J. 1994 Laser doppler measurement of turbulence parameters in a two-dimensional plane wall jet. *Phys. Fluids* **6** (9), 3116–3129.

Schober, M. & Fernholz, H.-H. 2000 Turbulence control in wall jets. *Eur. J. Mech., B/Fluids* **19** (4), 503–28.

Tutkun, M., George, W. K., Delville, J., Stanislas, M., Johansson, P. B. V., Foucaut, J.-M. & Coudert, S. 2009 Two-point correlations in high reynolds number flat plate turbulent boundary layers. *J. Turb.* **10**, N21.

Wygnanski, I., Katz, Y. & Horev, E. 1992 On the applicability of various scaling laws to the turbulent wall jet. *J. Fluid Mech.* **234**, 669–690.

Zhou, M. D., Heine, C. & Wygnanski, I. 1993 The forced turbulent wall jet in an external stream. In *3rd Shear Flow Conference*.

Zhou, M. D., Heine, C. & Wygnanski, I. 1996 The effects of excitation on the coherent and random motion in a plane wall jet. *J. Fluid Mech.* **310**, 1–37.

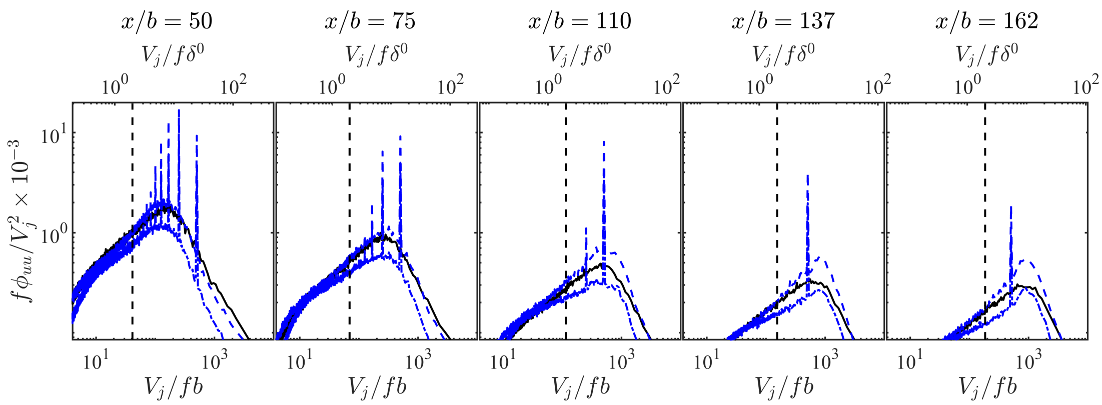

Figure 6. Compares the wall layer profiles ($z^+ \approx 15$ (-·-·-), $z^+ \approx 60$ (- - -)) of the pre-multiplied, one-dimensional, streamwise energy spectra $f\phi_{uu}$ corresponding to the perturbed flow with that of the outer layer ($z \approx 0.6\delta^0$ (–)) of the unperturbed flow. The vertical line shows the wavelength discriminator $\lambda_x = 2\delta^0$ (- - -)

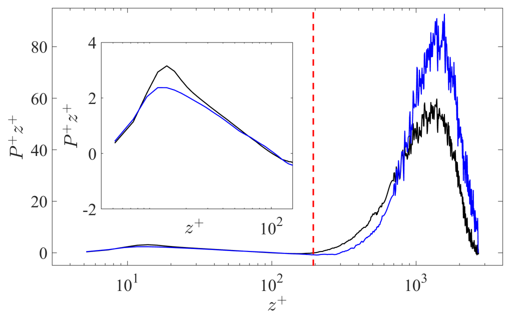

Figure 7. Compares the pre-multiplied production Pz of the unperturbed (–) and the unperturbed (–) flow. The vertical line (- - -) shows the wall-normal location z_m of the maximum velocity U_m corresponding to the unperturbed flow.

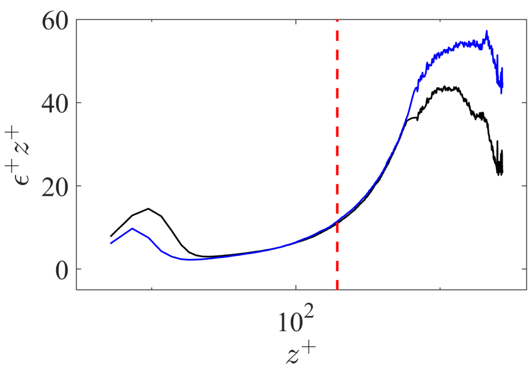

Figure 8. Compares the pre-multiplied dissipation rate εz of the unperturbed (–) and the unperturbed (–) flow. The vertical line (- - -) shows the wall-normal location z_m of the maximum velocity U_m corresponding to the unperturbed flow.